

Control Volume-Radial Basis Function Solution of 2D Driven Cavity Flow in Terms of the Velocity Vorticity Formulation

C. A. Bustamante¹, W. F. Florez¹, H. Power², M. Giraldo¹ and A. F. Hill¹

Abstract: The two-dimensional Navier Stokes system of equations for incompressible flows is solved in the velocity vorticity formulation by means of the Control Volume-Radial Basis Function (CV-RBF) method. This method is an improvement to the Control Volume Method (CVM) based on the use of Radial Basis Function (RBF) Hermite interpolation instead of the classical polynomial functions. The main advantages of the CV-RBF method are the approximation order, the meshless nature of the interpolation scheme and the presence of the PDE operator in the interpolation. Besides, the vorticity boundary values are computed in terms of the values of the velocity field at the neighbouring nodal points according to its definition by applying the curl operator to the local velocity interpolation function. Several interpolation strategies are tested for both the velocity and vorticity fields. A Newton type algorithm is implemented to solve the coupled system of non linear equations. As test example, the proposed numerical scheme is used to solve the lid driven cavity flow problem up to $Re = 5000$, where high Reynolds number solutions are achieved by using a Conservative and Hermitian interpolation for the velocity field.

Keywords: Local Hermite interpolation, Radial Basis Function, velocity vorticity, Control Volume Method.

1 Introduction

Several strategies have been implemented to lower the truncation error of the approximations used for interpolating the convective and diffusive fluxes in the Control Volume Method (CVM) discretization [Ye, Mittal, Udaykumar, and Shyy (1999); Vidovic, Segal, and Wesseling (2004); Perron, Boivin, and Herard (2004)]. Conventional CVM interpolation schemes present difficulties when they are applied

¹ Universidad Pontificia Bolivariana, Medellin, Antioquia, Colombia.

² University of Nottingham, Nottingham, Nottinghamshire, UK.

on domains with curved borders due to its inherent dependency on mesh configuration. Regarding high order approximations for convective fluxes in complex geometries, Abgrall (1994) studies flux reconstruction on very irregular unstructured meshes by two-dimensional polynomial functions in hyperbolic equations. With the same aim Jayantha and Turner (2005) use Least Squares Reconstruction Technique (LSRT), while Truscott and Turner (2004) and Manzini and Putti (2007) resort to Gauss-Green Gradient Reconstruction Technique (GGRT) for computing the diffusive fluxes and LSRT approximation for convective ones. In order to maintain adequate processing times and to reduce dependency on mesh, other strategies need to be implemented and tested.

One possible alternative to improve the accuracy of the evaluation of surface fluxes is the use of radial basis function (RBF) interpolations. In the literature, the RBF interpolation method is considered as an optimal numerical technique for interpolating multidimensional scattered data. Although most work done so far on RBF relates to scattered data approximation and, in general, to interpolation theory. There has recently been an increased interest in the use of RBF as the base of meshless collocation approaches for solving partial differential equations (PDEs). The use of RBF interpolation technique has become the foundation of the RBF Meshless Collocation Methods for the solution of Partial Differential Equations, since the pioneer work on the unsymmetric method by Kansa (1990). Kansa's approach is based on an intrinsic relationship between the interpolation scheme and the differential equations to be solved [Kansa and Hon (2000)]. Instead of using a direct interpolation scheme, as in the unsymmetric approach, Fasshauer (1997) proposed the symmetric approach based on a Hermite interpolation, where the RBFs besides interpolating a given function can also approximate or reconstruct its spatial derivatives, resulting in better accuracy than the unsymmetric method. LaRocca, Hernandez, and Power (2005) use the symmetric scheme to solve the convection diffusion equation, and LaRocca and Power (2008) implement a double collocation strategy in the symmetric scheme to improve the numerical solution towards the boundary, where at the boundary collocation points beside imposing the boundary condition the governing equation (PDE) is also satisfied.

Although full-domain RBF methods are highly flexible and exhibit high order convergence rates [Madych and Nelson (1990)], the fully-populated matrix systems they produce lead to poor numerical conditioning as the size of the data-set increases. This problem is described by Schaback (1995) as the uncertainty relation; better conditioning is associated with worse accuracy, and worse conditioning is associated with improved accuracy. As the system size is increased, this problem becomes more pronounced. Many techniques have been developed to reduce the effect of the uncertainty relation, such as RBF-specific preconditioners [Brown (2005)], and adaptive selection of data centres [Ling and Schaback (2004)]. How-

ever, at present the only reliable method of controlling numerical ill-conditioning and computational cost as problem size increases is through domain decomposition (see, for example, Lee, Liu, and Fan (2003); Sarler and Vertnik (2006); Divo and Kassab (2006), and Wright and Fornberg (2006)).

The idea of introducing RBF interpolation to improve the accuracy of a classical numerical scheme has been recently employed by Wright and Fornberg (2006). In this work the authors utilize a Hermitian RBF interpolation to remove the symmetry constraint required to achieve high order approximation in the FD scheme. In the context of the CV unstructured mesh approach, Moroney and Turner (2006) and (2007) improved Liu, Turner, and Anh (2002) CV approach which uses FE polynomial shape functions, for 2D and 3D problems respectively. Moroney and Turner's approach relies on a local RBF interpolation of the field variable, instead of the FE polynomials functions, where the CV centres of the considered stencil act as trail points. In particular, Moroney and Turner consider the ability of their CV-RBF scheme to achieve high accuracy on relatively coarse meshes due to the high accuracy of the RBF interpolation to evaluate derivatives [Madych (1992); Fornberg and Flyer (2005)] and thus guaranty a high order approximation of the diffusive flux. Moroney and Turner validated their new approach by solving different scalar transport problems, observing significant in the improvement the estimation of the diffusion fluxes.

Following Moroney and Turner (2007) and (2006) ideas, Orsini, Power, and Morovan (2008) also used RBF interpolations to improve the accuracy of classical CV schemes. Their method is based on a local RBF interpolation of the field variable at the control volume cell centres, as in the case of Moroney and Turner CV-RBF approach, but in their approach they also require that the local interpolation satisfies the governing equation at a set of auxiliary interpolation points and the boundary conditions at local interpolation systems containing boundary points, i.e. the used interpolation functions are also approximation of the governing equation found by the use of a local RBF meshless collocation scheme with the boundary conditions directly imposed at the local level. Both the unsymmetric and symmetric RBF meshless approaches were used and their results compared.

Several scalar convective-diffusion problems were considered by Orsini, Power, and Morovan (2008) to test the proposed CV-RBF approach, showing the corresponding improvement on the estimation of convective and diffusion fluxes. In their implementation they use central defined interpolation stencils without the need of any upwinding scheme, since their approach provides a form of analytical upwinding given by the interpolation coefficients, found by the solution of the local boundary value problem, which retain the desired information about the convective velocity field (for more details about the stability of this type of CV-RBF approach see Orsini, Power, Morovan, and Lees (2010)).

In this type of CV-RBF approach, at the local interpolation the RBF strong form formulation is used while the CV weak form is employed to solve the global problem. In this way, the best features of the two approaches are used, avoiding the ill-conditioning issues of the global RBF meshless approach for large number of trial and collocation points. Besides, the use of localised RBF for reconstruction step in CV resolves the ill-conditioning issues encountered in Abgrall (1994) and Dumbser and Kaser (2007) for the computation of the polynomial coefficients. In fact, choosing the RBF type appropriately and limiting the number of collocation points used lead to an interpolation that is well posed in all dimensions.

In this work, the CV-RBF approach proposed by Orsini, Power, and Morovan (2008) is implemented to solve 2D Navier-Stokes flow problems in terms of its velocity-vorticity formulation, with application to driven cavity flow. The main difficulty encountered in the present case is the solution at the local level of the system of coupling nonlinear PDEs, to define the required interpolation functions. For this reason, we consider several alternatives for the local interpolations, which are tested and compared.

The velocity-vorticity formulation is used to avoid the problem of the pressure-velocity coupling in incompressible fluid flow. In this type of formulation, the flow kinetics is determined by a convective-diffusion PDE for the vorticity component while flow kinematics is defined by a Poisson PDE equation coupling the velocity and vorticity fields. In order to solve the kinetics equation, the boundary vorticity values must be known [Skerget and Rek (1995); Young, Liu, and Eldho (2000); Hribersek and Skerget (2005); Zunic, Hribersek, Skerget, and Ravnik (2007)]. Therefore, the kinematics and kinetics are solved sequentially. Qian and Vezza (2001) consider vorticity generation through the domain boundaries in the unsteady situation. The velocity vorticity formulation can be solved in a coupled way by linking the boundary vorticity values with the velocity nodal values. Lo, L.Young, and Tsai (2007) generate a coupled system of equations by employing the Differential Quadrature (DQ) method for spatial discretization.

Several numerical techniques have been reported in the literature to solve viscous flow problems in terms of their velocity-vorticity formulation (see for example, Skerget and Rek (1995) where a BEM is used, Huang and Li (1997) a FDM and Young, Liu, and Eldho (2000) a FEM-BEM coupled scheme). More recently, Hribersek and Skerget (2005) deal with complex geometry situations by the Boundary Domain Integral Method (BDIM) for high Reynolds numbers. Zunic, Hribersek, Skerget, and Ravnik (2007) use the scheme implemented by Young, Liu, and Eldho (2000) for three-dimensional domains. With a similar formulation Pascazio and Napolitano (1996) solve the Navier Stokes equations for transient flow in staggered grids, where velocities are known at the volume faces and the vorticities at the nodes. Qian and Vezza (2001) apply CVM to solve the kinetics equation and

the Bio-Savart Law to compute velocities in an iterative time marching algorithm. They also used an additional scheme to compute vorticity values at boundaries. Among others, these are some examples of previously works published in the literature using the velocity-vorticity formulation.

In this paper the vorticity transport (kinetics) and Kinematics Poisson equations are solved using the Newton Raphson method. In the first part of this paper the velocity vorticity formulation is presented, then the CVM discretization are described and the different possibilities for the velocity and vorticity interpolation are explained. Afterwards the discretized CV-RBF expressions for the Navier Stokes equations are obtained and the developed algorithm to solve the coupled Navier Stokes system, in terms of its velocity-vorticity formulation, is detailed. Finally the results for lid-driven cavity flow at $Re = 100, 400$ and 1000 are considered, where the different interpolation strategies are tested. The best interpolation strategy is then used to solve the problem up to $Re = 5000$. The $Re = 5000$ is a good test case, since the steady state solution still stable but not too far from the first Hopf bifurcation (for more details see Bruneau and Saad (2006)). All the obtained numerical results are compared with benchmark solutions previously reported in the literature, showing excellent comparison even with the use of relative coarse meshes.

2 Velocity vorticity formulation

The incompressible velocity vorticity formulation is found by applying the curl operator to the Navier Stokes system of equations in terms of the primitive variables. Substituting the definition of the vorticity field as the curl of the velocity field, Eq. (1), into the resulting equation a transport equation for the vorticity field is obtained (see Skerget and Rek (1995)). Equations (2) and (3), given below, express the vorticity transport (kinetics) and the mass conservation equations for steady state two-dimensional flows, in terms of a dimensionless vorticity component in x_3 direction ω and a dimensionless velocity field u_i with $i = 1, 2$, where Re and e_{3ij} are the Reynolds number and the component in the $k = 3$ direction of the pseudo scalar constant, respectively.

$$\omega = e_{3ij} \frac{\partial u_i}{\partial x_j} \quad (1)$$

$$\frac{\partial^2 \omega}{\partial x_j \partial x_j} - Re u_j \frac{\partial \omega}{\partial x_j} = 0 \quad (2)$$

$$\frac{\partial u_i}{\partial x_i} = 0 \quad (3)$$

Applying the curl operator to vorticity definition (1) and considering the mass conservation constraint (3), the following Poisson equation for the velocity field is found, (4).

$$\frac{\partial^2 u_i}{\partial x_j \partial x_j} + e_{3ij} \frac{\partial \omega}{\partial x_j} = 0 \quad (4)$$

Equations (2) and (4) represent the kinetic and kinematic counterparts of the original Navier-Stokes system and define the system of equations to be solved in our formulation. In the present work, we are only considering boundary conditions of the Dirichlet type, i.e. given boundary velocity (5). However, our formulation can be easily extended to other types of boundary conditions.

$$u_i = c_i(\vec{x}) \quad (5)$$

In the present case, it is not necessary to know the values of the boundary vorticity beforehand, since they can be computed from the definition (1) and expressed in terms of the unknown internal and the prescribed boundary velocity values.

3 Control Volume-Radial Basis Function Method (CV-RBF)

The CV-RBF approach differs from classical CVM in the way that the flux at the cell surfaces is computed. A local RBF interpolation of the field variable is performed at the cell centres that define a local stencil used to obtain the shape function at the integration cell, from which the fluxes are determined. In addition, it is required that such interpolation satisfies the governing equations (PDEs) in a certain number of points inside the considered stencil. In this way, the local interpolating function is given by an approximated solution of the original PDEs. To find the solution to the local problems, both the unsymmetric (Kansa's method) and symmetric (Hermitian method) RBF approaches can be used. Besides, by using the RBF interpolation scheme it is guaranteed high order accuracy in the approximation of derivatives [Fornberg and Flyer (2005)]. In the following section, the system of equations is discretized according to the traditional CVM approach. Afterwards the different strategies to apply the RBF interpolation are explained and the final discrete expressions of the CV-RBF method are presented.

3.1 CVM discretization

The system of equations (2) and (4) is expressed as (6) and (7) after integrating over a control volume V and applying Gauss' Theorem. The surface S is the boundary of V and \vec{n} the unit outward normal vector.

$$\int_S \frac{\partial \omega}{\partial x_j} n_j dS - \int_S Re \omega u_j n_j dS = 0 \quad (6)$$

$$\int_S \frac{\partial u_i}{\partial x_j} n_j dS + \int_S \omega e_{3ij} n_j dS = 0 \quad (7)$$

In two-dimensional, the control volume is consider as a polygon of N_s sides, and the surface S is the total length by the polygon sides. Hence, each surface integral in the above equations can be expressed as the sum of integrals over each side. To get the final expressions a numerical scheme must be applied to approximate the surface integrals. For simplicity, the mid-value integral approach is used to obtain the discrete equations (8) and (9).

$$\sum_{l=1}^{N_s} \left(\frac{\partial \omega}{\partial x_j} n_j \Delta S_l \right)_{\vec{x}=\vec{x}_l} - \sum_{l=1}^{N_s} (Re \omega u_j n_j \Delta S_l)_{\vec{x}=\vec{x}_l} = 0 \quad (8)$$

$$\sum_{l=1}^{N_s} \left(\frac{\partial u_i}{\partial x_j} n_j \Delta S_l \right)_{\vec{x}=\vec{x}_l} + \sum_{l=1}^{N_s} (\omega e_{3ij} n_j \Delta S_l)_{\vec{x}=\vec{x}_l} = 0 \quad (9)$$

To find the final discrete system of equations, it is required to approximate the values of the field variables and their directional derivatives at the CV face centre points in terms of the cell nodes field values, where the cell nodes are located at the control volumes geometric centre.

3.2 RBF Hermitian interpolation scheme

The RBFs only depend on the Euclidean distance between a subset of trial centres $\vec{\xi}_j$ and a field point \vec{x} (collocation point). There are several types of RBFs that can be used in the interpolation [LaRocca, Hernandez, and Power (2005)], in this work the Multiquadric function (MQ) defined by (10) is used.

$$\Psi(r) = (r^2 + c^2)^{m/2} \quad (10)$$

where $r = |\vec{x} - \vec{\xi}_j|$ is the Euclidean distance between a collocation point, \vec{x} , and a trial point, $\vec{\xi}_j$, and m is an integer number. The MQ function has a free shape parameter c which controls the shape of the interpolation surface around the field point. When c decreases the interpolation surface tends to the shape of a cone basis function, while as it increases the cone peak gradually flattens. Currently, the strategies to find the optimal c is a topic of active research. However, some simple strategies can help in its selection [Huang, Lee, and Cheng (2007)]. Besides, the MQ is a conditionally positive definite function of order m , which require the addition of a polynomial term of order $m - 1$ together with a homogeneous constraint condition in order to obtain an invertible interpolation matrix. It is also well known, that exponentially convergence can be achieved by a MQ direct interpolation algorithm (for more details see Madych and Nelson (1990)).

Let consider a given boundary value problem expressed by the linear partial differential operators L and B , which are apply to a field variable ϕ in the domain, equation (11), and on the boundary, equation (12), respectively.

$$L[\phi(\vec{x})] = f(\vec{x}) \tag{11}$$

$$B[\phi(\vec{x})] = g(\vec{x}) \tag{12}$$

According to the Hermitian interpolation scheme (Symmetric method [Jumarhon, Amini, and Chen (2000)]), the solution ϕ of the above boundary value problem can be expressed as in (13), where n is the number of boundary points, $N - n$ is the number of internal collocation centres and the operator subindex ξ refers to the derivative variable.

$$\phi(\vec{x}) = \sum_{j=1}^n \alpha_j B_{\xi}[\Psi(\|\vec{x} - \vec{\xi}_j\|)] + \sum_{j=n+1}^N \alpha_j L_{\xi}[\Psi(\|\vec{x} - \vec{\xi}_j\|)] + \sum_{j=1}^{NP} \alpha_{j+N} P_{m-1}^j(\vec{x}) \tag{13}$$

By substituting the approximated function ϕ into the governing equation (11), (PDE), and the boundary conditions (12), and evaluating them at the $N - n$ internal points and n boundary points, respectively, the following linear algebraic system of equations, (14), is obtained:

$$\begin{pmatrix} B_x B_{\xi}[\Psi] & B_x L_{\xi}[\Psi] & B_x [P_{m-1}] \\ L_x B_{\xi}[\Psi] & L_x L_{\xi}[\Psi] & L_x [P_{m-1}] \\ B_x [P_{m-1}^T] & L_x [P_{m-1}^T] & 0 \end{pmatrix} (\alpha) = \begin{pmatrix} g(\vec{x}) \\ f(\vec{x}) \\ 0 \end{pmatrix} \tag{14}$$

The resulting interpolation matrix is non-singular, as long as linearly dependent operators are collocated at different locations, [Orsini, Power, and Morovan (2008)]. Besides, the obtained interpolation matrix is symmetric. A notorious feature of the Hermite interpolation scheme is that the resulting interpolation coefficients α contains information about the PDE operator, that defines the physical phenomena (more details about the Symmetric method can be found in LaRocca and Power (2008)).

3.3 CV-RBF discretization

Unlike in the global RBF meshless numerical scheme [LaRocca, Hernandez, and Power (2005)], in the CV-RBF method a local RBF interpolation is implemented at a small subdomain (interpolation stencil) placed on each computational cell (control volume), including their neighbouring cells. There are many possibilities to define the stencil configuration in relation to the grid used. Orsini, Power, and Morovan (2008) tested two different configurations for the CV-RBF solution of convection-diffusion problems; the *one stencil one cell* (Figure 1 a.), where each

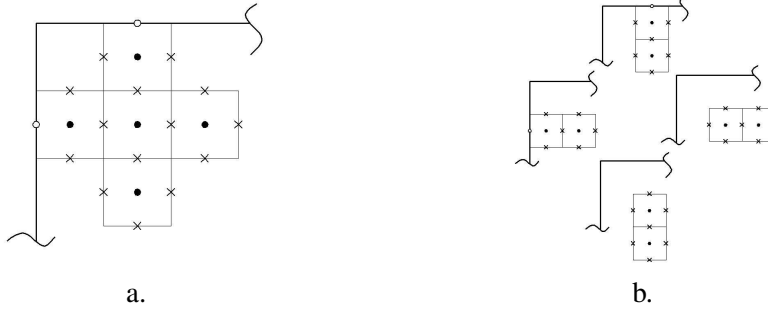


Figure 1: Stencil configurations: a. One stencil one cell, b. One stencil one face

subdomain is made of each control volume and its neighbours, and the *one stencil one face* (Figure 1 b.), in which a subdomain is defined for each cell face. More accurate results were obtained with the use of the first configuration. In the present work, the *one stencil one cell* configuration is chosen as the interpolation stencil. As shown in Figure 1, three types of trial and test points (in this case located at the same places) are used. They are group in p nodal points (●), the centre of CVs included in the stencil where the unknown field variable is interpolated, n boundary locations (◦), in the case when the interpolation stencil include the problem boundary where the boundary condition is to be satisfied, and $N - n - p$ PDE points (×), where the PDE is satisfied by the Hermite interpolation. Once the stencil configuration is set, an interpolation function is defined.

In the present case of incompressible two-dimensional stationary viscous fluid flow problem, the following set of linear partial differential operators can be defined.

$$L_x() = \frac{\partial^2()}{\partial x_j \partial x_j} \quad (15)$$

$$M_x() = \frac{\partial^2()}{\partial x_j \partial x_j} - Re u_j^* \frac{\partial}{\partial x_j} \quad (16)$$

$$D_{x_j}() = \frac{\partial}{\partial x_j} \quad (17)$$

The PDE linear operators L_x , M_x and D_{x_i} in expressions (15),(16) and (17) are obtained from the kinematics (4), kinetics (2), and continuity (3) equations, respectively, where the M_x operator is a linearized form of the vorticity equation (2) with the value of the velocity field \bar{u}^* approximated by its value at the previous iteration.

In this way, at the local level the following linearized PDEs are defined:

$$L_x(u_i) = e_{3ij} \frac{\partial \omega}{\partial x_j} \tag{18}$$

$$M_x(\omega) = 0 \tag{19}$$

$$D_{x_j}(u_i) = 0, \tag{20}$$

to be used in the local Hermite interpolation at each stencil.

In (18), the value of directional derivatives of the vorticity ω is defined by the derivatives of the vorticity interpolation function and given in terms of the local values of the vorticity at the stencil interpolation nodes. At those stencils having boundary points, the boundary operator $B_x(\cdot) = (\cdot)$ is defined by the velocity or vorticity boundary value according to the corresponding governing equation. The implementation of these two types of boundary conditions is described in details in the next paragraphs.

Two variables need to be represented in terms of a RBF interpolation in the above local formulation. With the aim of looking at the best interpolation scheme, a combination of four strategies for the velocity and two for the vorticity are developed and tested.

The first case is a simple interpolation (SI), in which the dependent variable is approximated by a direct RBF interpolation with collocation at the nodal centres and boundary points, i.e. no PDE operators are used neither in the interpolation formula nor in the collocation process.

$$\theta(\vec{x}) = \sum_{j=1}^p \alpha_j \Psi(\|\vec{x} - \vec{\xi}_j\|) + \sum_{p+1}^n \alpha_j B_\xi [\Psi(\|\vec{x} - \vec{\xi}_j\|)] + \sum_{N+1}^{NP} \alpha_j P_{m-1}^j \tag{21}$$

$$\sum_{j=1}^p \alpha_j P_{m-1}^k(x_j) + \sum_{j=p+1}^{p+n} \alpha_j B_x [P_{m-1}^k(x_j)] = 0 \quad k = 1, 2, \dots, NP \tag{22}$$

In (21), the approximated variable θ can be the velocity components or the vorticity and Ψ is the RBF related to each variable. In this case the boundary operator B_x is the unit operator for both the velocity and vorticity components, where the vorticity boundary values are defined in terms of the unknown and prescribed velocity values at the interpolation stencil, by taking the curl of the velocity interpolation function and reconstructing its value at the boundary points.

The interpolation matrix system (23) is obtained by evaluating the RBF approximation (21) at each collocation point of the stencil considered, i.e. the nodal and

boundary points, together with the homogeneous constraint condition for the polynomial term (22), resulting in a symmetric matrix system.

$$\begin{pmatrix} \Psi & B_\xi[\Psi] & P_{m-1} \\ B_x[\Psi] & B_x B_\xi[\Psi] & B_x[P_{m-1}] \\ P_{m-1}^T & B_x[P_{m-1}^T] & 0 \end{pmatrix} (\alpha_i) = \begin{pmatrix} (\bar{\theta})_{cells} \\ g(\vec{x}) \\ 0 \end{pmatrix} \quad (23)$$

For the velocity interpolation, $\theta = u_i$, $[g(\vec{x})] = [c_i(\vec{x})]$ and the system of equations is written as $[A_i][\alpha_{(i)}] = [B_i]$. In case of the vorticity interpolation $\theta = \omega$, $[g(x)] = [e_{3ij} \frac{\partial u_i}{\partial x_j}]$ and the resultant system of equation is expressed as $[C][\beta] = [D]$. As before, in this case the directional derivative of the velocity field in the $[g(x)]$ vector term of the vorticity interpolation are defined in terms of the unknown velocity values by taking the curl of the velocity interpolation function and reconstructing its value at the nodal points.

A second alternative is to use the RBF Hermitian interpolation (HI) proposed by Orsini et al. for their CV-RBF scheme, [Orsini, Power, and Morovan (2008)]. The HI approximation is applied to the dependent variable by using the expression (24), which includes the PDE centres and the PDE operator N_x . For the velocity components the operator $N_x \equiv L_x$ while for the vorticity interpolation $N_x \equiv M_x$. The M_x operator implies a double iteration strategy that will be discussed in the next section, given that a linear approximation is used at the local level.

$$\begin{aligned} \theta(\vec{x}) = & \sum_{j=1}^p \alpha_j \Psi(\|\vec{x} - \vec{\xi}_j\|) + \sum_{j=p+1}^n \alpha_j B_\xi[\Psi(\|\vec{x} - \vec{\xi}_j\|)] \\ & + \sum_{j=p+n+1}^{N-p-n} \alpha_{j(i)} N_\xi[\Psi_i(\|\vec{x} - \vec{\xi}_j\|)] + \sum_{j=N+1}^{NP} \alpha_j P_{m-1}^j \end{aligned} \quad (24)$$

After collocation at the nodal, boundary and PDE centres, and completing the resulting matrix system with the corresponding homogeneous constraint condition, the following linear system of equations is obtained:

$$\begin{pmatrix} \Psi & B_\xi[\Psi] & N_\xi[\Psi] & P_{m-1} \\ B_x[\Psi] & B_x B_\xi[\Psi] & B_x N_\xi[\Psi] & B_x[P_{m-1}] \\ N_x[\Psi] & N_x B_\xi[\Psi] & N_x N_\xi[\Psi] & N_x[P_{m-1}] \\ P_{m-1}^T & B_x[P_{m-1}^T] & N_x[P_{m-1}^T] & 0 \end{pmatrix} (\alpha) = \begin{pmatrix} (\bar{\theta})_{cells} \\ g(\vec{x}) \\ f(\vec{x}) \\ 0 \end{pmatrix} \quad (25)$$

Like in the SI scheme, the resultant system is written as $[A_i][\alpha_{(i)}] = [B_i]$ for the velocity components and $[C][\beta] = [D]$ for the vorticity. According to equations (18)

and (19), the free term in the RHS column vector corresponding to the PDE centres, is given by $[f(\vec{x})] = [-e_{3ij} \frac{\partial \omega}{\partial x_j}]$ for the velocity, which is defined in terms of the nodal values of the vorticity field according to the used interpolation scheme, and $[f(\vec{x})] = [0]$ for the vorticity. If in (24) and (25) the boundary and PDE operators, i.e. B_ξ and N_ξ respectively, are defined by the identity operator, the above scheme reduces to the un-symmetric or Kansa's method [Kansa (1990)]. As can be observed from the used interpolation scheme, the obtained interpolation coefficients for the velocity and vorticity are function of both the velocity and vorticity stencil nodal values, strongly coupling both variables.

The continuity equation is not explicit imposed in the velocity-vorticity formulation, which is based on a Poisson like expression for kinematics, consequently it is not possible to guarantee that mass conservation can be satisfied in the whole domain [Dworkin, Bennett, and Smooke (2006)]. As an alternative, the conservative interpolation (CI) proposed by Florez and Power (2002) is implemented for the velocity approximation as the third option. According to the CI interpolation, the velocity approximation is defined by the expression (26).

$$u_i(\vec{x}) = \sum_{j=1}^p \alpha_{j(i)} \Psi(\|\vec{x} - \vec{\xi}_j\|) + \sum_{j=p+1}^n \beta_{j(i)} B_\xi [\Psi(\|\vec{x} - \vec{\xi}_j\|)] + \sum_{j=p+n+1}^{N+n} \gamma_j D_{\xi_i} [\Psi(\|\vec{x} - \vec{\xi}_j\|)] + \sum_{j=N+n+1}^{NP+N+n} \zeta_{j(i)} P_{m-1}^j \quad (26)$$

Besides collocating the velocity values at nodal and boundary centres, the continuity operator is also applied at the boundary and PDE nodes, imposing there the mass conservation equation. After coupling the interpolation matrices for the velocity components according with the mass conservation equation, i.e. divergent free for incompressible flow, the system of equations (27), $[A][\alpha] = [B]$, is obtained. In this way, the interpolation coefficients for each velocity component are given in terms of the unknown velocity values at the nodal centres, i.e. CV centres.

The fourth interpolation option, which applies only for the velocity approximation, is a combination between the Conservative and Hermitian interpolation (CHI). A coupled interpolation matrix is obtained in a similar way of equation (27), now considering the L differential operator both in the approximation function and the collocation process. As in the CI case, the interpolation coefficients will be obtained in terms of both velocity components.

Regardless of the option, the interpolation coefficients are given in terms of the respective field variables which are listed in the vectors $\vec{\omega}_{cells}$ and $(\vec{u}_i)_{cells}$. After inverting the interpolation matrices A_i (or A in the CI and CHI cases) and C the velocity, the vorticity and their derivatives can be found in any location of the stencil

in terms of the velocity and vorticity values at the stencil nodes.

$$\left(\begin{array}{ccccccc} \Psi & B_{\xi}^1[\Psi] & D_{\xi_1}[\Psi] & 0 & 0 & [P_1^{m-1}] & 0 \\ B_x^1[\Psi] & B_x^1 B_{\xi}^1[\Psi] & B_x^1 D_{\xi_1}[\Psi] & 0 & 0 & B_x^1 [P_1^{m-1}] & 0 \\ D_{x_1}[\Psi] & D_{x_1} B_{\xi}^1[\Psi] & D_{x_j} D_{\xi_j}[\Psi] & D_{x_2}[\Psi] & D_{x_2} B_{\xi}^2[\Psi] & D_{x_1} [P_1^{m-1}] & D_{x_2} [P_2^{m-1}] \\ 0 & 0 & D_{\xi_2}[\Psi] & \Psi & B_{\xi}^2[\Psi] & 0 & P_2^{m-1} \\ 0 & 0 & B_x^2 D_{\xi_2}[\Psi] & B_x^2[\Psi] & B_x^2 B_{\xi}^2[\Psi] & 0 & B_x^2 [P_2^{m-1}] \\ (P_1^{m-1})^T & B_x^1 [P_1^{m-1}]^T & D_{x_1} [P_1^{m-1}]^T & 0 & 0 & 0 & 0 \\ 0 & 0 & D_{x_2} [P_2^{m-1}]^T & [P_2^{m-1}]^T & B_x^2 [P_2^{m-1}]^T & 0 & 0 \end{array} \right) \begin{pmatrix} \alpha_1 \\ \beta_1 \\ \gamma \\ \alpha_2 \\ \beta_2 \\ \zeta_1 \\ \zeta_2 \end{pmatrix} = \begin{pmatrix} \bar{u}_{1,cells} \\ c_1(\vec{x}) \\ 0 \\ \bar{u}_{2,cells} \\ c_2(\vec{x}) \\ 0 \\ 0 \end{pmatrix} \quad (27)$$

According to expressions (8) and (9), the velocity and vorticity fields as well as their normal derivatives at the cell face centres \vec{x}_l are required to be given in terms of the velocity and vorticity values at the stencil nodes, i.e. centres of the CV. For the SI and HI approximations, the interpolation functions evaluated at cell face centres can be calculated as follows by means of the following vector products.

$$u_i|_{\vec{x}=\vec{x}_l} = \bar{E}_{(i)}^T|_{\vec{x}=\vec{x}_l} \vec{\alpha}_i \quad (28)$$

$$\omega|_{\vec{x}=\vec{x}_l} = \bar{F}^T|_{\vec{x}=\vec{x}_l} \vec{\beta} \quad (29)$$

$$\frac{\partial u_i}{\partial x_j}|_{\vec{x}=\vec{x}_l} = \frac{\partial \bar{E}_{(i)}^T}{\partial x_j}|_{\vec{x}=\vec{x}_l} \vec{\alpha}_i \quad (30)$$

$$\frac{\partial \omega}{\partial x_j}|_{\vec{x}=\vec{x}_l} = \frac{\partial \bar{F}^T}{\partial x_j}|_{\vec{x}=\vec{x}_l} \vec{\beta} \quad (31)$$

where the components of the vector \bar{E}_i^T and \bar{F}^T in the above equations depend on the used interpolation option. For instance in the HI the vectors are:

$$\bar{E}_i^T = \left(\left[\Psi_i(\|\vec{x} - \vec{\xi}_j\|) \right], \left[B_{\xi} \Psi_i(\|\vec{x} - \vec{\xi}_j\|) \right], \left[L_{\xi} \Psi_i(\|\vec{x} - \vec{\xi}_j\|) \right], P_{m-1}(\vec{x}) \right) \quad (32)$$

$$\bar{F}^T = \left(\left[\Phi(\|\vec{x} - \vec{\xi}_j\|) \right], \left[B_{\xi} \Phi(\|\vec{x} - \vec{\xi}_j\|) \right], \left[M_{\xi} \Phi(\|\vec{x} - \vec{\xi}_j\|) \right], P_{m-1}(\vec{x}) \right) \quad (33)$$

In the CI case the velocity components can be interpolated by using the expression (34), where the vectors $\bar{G}_{(1)}^T$ and $\bar{G}_{(2)}^T$ are given by equations (35) and (36), while the vector $[\Lambda]$ is defined as the array of the unknown interpolation coefficient. For the CHI approximation the reconstruction is done in a similar way.

$$u_i|_{\vec{x}=\vec{x}_i} = \bar{G}_{(i)}^T \Big|_{\vec{x}=\vec{x}_i} \vec{\Lambda} \tag{34}$$

$$\begin{aligned} \bar{G}_1^T = & \left(\left[\Psi(\|\vec{x} - \vec{\xi}_j\|) \right], \left[B_\xi^1 \Psi(\|\vec{x} - \vec{\xi}_j\|) \right], D_{\xi_1} \left[\Psi(\|\vec{x} - \vec{\xi}_j\|) \right], [0], [0], P_1^{m-1}(\vec{x}), [0] \right) \end{aligned} \tag{35}$$

$$\begin{aligned} \bar{G}_2^T = & \left([0], [0], D_{\xi_2} \left[\Psi(\|\vec{x} - \vec{\xi}_j\|) \right], \left[\Psi(\|\vec{x} - \vec{\xi}_j\|) \right], \left[B_\xi^2 \Psi(\|\vec{x} - \vec{\xi}_j\|) \right], [0], P_2^{m-1}(\vec{x}) \right) \end{aligned} \tag{36}$$

The CV-RBF discretization process is completed by substituting the reconstruction expressions in the CV equations (8) and (9) and expressing the interpolation coefficients in terms of the nodal field values defined by the vectors B_i (or B in the CI and CHI cases) and D . This process leads to the discrete Navier Stokes system of equations in terms of the stencil nodal values of velocity and vorticity. In case of SI and HI interpolation, the resultant equations are given by equations (37) and (38).

$$\sum_{l=1}^{N_s} \left(\frac{\partial \bar{F}^T}{\partial x_j} n_j \Delta S \right)_{\vec{x}=\vec{x}_i} C^{-1} D - \sum_{l=1}^{N_s} (Re \bar{F}^T)_{\vec{x}=\vec{x}_i} C^{-1} D (\bar{E}_j^T n_j \Delta S)_{\vec{x}=\vec{x}_i} A_{(j)}^{-1} B_{(j)} = 0 \tag{37}$$

$$\sum_{l=1}^{N_s} \left(\frac{\partial \bar{E}_i^T}{\partial x_j} n_j \Delta S \right)_{\vec{x}=\vec{x}_i} A_{(i)}^{-1} B_{(i)} + \sum_{l=1}^{N_s} (\bar{F}^T e_{3ij} n_j \Delta S)_{\vec{x}=\vec{x}_i} C^{-1} D = 0 \tag{38}$$

When those expressions are applied to each stencil, a $3m \times 3m$ non-linear system of equations is obtained, i.e. the nodal values of the two velocity components and the vorticity field. For a given interpolation option, the obtained nonlinear system of equations is solved by employing the algorithm presented in the next section.

4 Solution algorithm

The CVRBF numerical solution of the 2D Navier Stokes system of equations in terms of its velocity and vorticity formulation is solved by means of a recursive algorithm given by a Newton-Raphson iterative scheme to deal with the obtained

global non-linear system of algebraic equations. One of the main difficulty in this type of formulation is the evaluation of the unknown boundary condition for the vorticity field that requires a sequential solution procedure [Skerget and Rek (1995)]. In this case the sequential computation is avoided by expressing the vorticity boundary values in terms of the unknown internal and prescribed boundary nodal values of the velocity field at the boundary interpolation stencils, obtained from the differentiation of the used velocity interpolation scheme according to the definition of the vorticity.

Before describing the proposed numerical algorithm, it is necessary to explain the use of the different interpolation strategies for the field variables described previously: The first strategy is to use the SI interpolation for both the velocity and the vorticity fields (SI-SI). The second one employs the HI interpolation for the velocities and SI for the vorticity (HI-SI) while the third strategy consists in using the CI interpolation for the velocity field and SI for the vorticity (CI-SI). The CHI approach is employed to interpolate the velocity field in conjunction with the SI interpolation for the vorticity in the fourth strategy (CHI-SI) and with the HI interpolation for the vorticity as the fifth strategy (CHI-HI).

As previously commented, at the local level the Hermitian interpolation is formulated in term of a simple Picard iteration scheme, where the convective term of the vorticity equation is linearized by using the value of the velocity field at the previous iteration, \vec{u}^* . In the proposed interpolation strategies only the CHI-HI approach requires updating of the interpolation matrices at each iteration, due to the linearization of the convective term of the vorticity PDE operator M_x . Therefore in the CHI-HI approach, the operators M_x and M_ξ in the interpolation matrix need to be updating at each iteration.

The numerical algorithm can be described as:

- Guess an initial velocity field \vec{u}^0 to be used in the linearization of the convective term of the HI local approximation of the vorticity equation and as initial value on the Newton-Raphson algorithm at the CV global solution.
- Compute the interpolation matrix $[C]$ and the column vector $[D]$. The vorticity boundary values in $[D]$ are calculated by reconstructing the velocity gradient according to the used velocity interpolation. Hence, the vector $[D]$ and the interpolation coefficients $[\beta]$ are expressed in terms of the unknown stencil nodal values of velocity and vorticity fields for the given values of the boundary velocity. In the CHI-HI strategy it is necessary to use the guess velocity value at PDE points to compute the interpolation matrix $[C]$, which are defined by the solution at the previous iteration.

- Find the interpolation matrix $[A]_i$ (or $[A]$, in the CI and CHI cases) and the column vector $[B]_i$ (or $[B]$). By solving the resulting linear system of equations, the interpolation coefficients are expressed in terms of the nodal velocity and vorticity values.
- Solve the system of equations (37) and (38) by means of the Newton Raphson iterative scheme until a desirable convergence is achieved, where the numerical Jacobian matrix is computed by using a second order finite difference approximation.
- In the SI-SI, CI-SI and CHI-SI strategies, the obtained values from the Newton-Raphson algorithm of $\bar{u}_{1\text{cells}}$, $\bar{u}_{2\text{cells}}$ and $\bar{\omega}_{\text{cells}}$ are the final solution. However in the CHI-HI scheme, the obtained velocity field is used to update the linearized operators M_x and M_ξ of the local interpolation matrices. With this new local approximation, the above steps are repeated until a tolerance criterion is achieved. The tolerance criterion is applied such that iteration stops if $\varepsilon_{RMS} < tol$, where ε_{RMS} is the Root Mean Square residual between velocity values at present and previous iteration.

5 Numerical results

The CV-RBF method with the interpolation strategies discussed above, were implemented in a FORTRAN 90 code. To test the accuracy of each of the proposed interpolation schemes, the steady state solution of a two-dimensional lid-driven cavity viscous flow is considered and the corresponding results compared with previous numerical solutions. To evaluate each of the interpolation schemes, results are obtained for Reynolds numbers 100, 400 and 1000 using the five proposed strategies (SI-SI, HI-SI, CI-SI, CHI-SI, CHI-HI). Next, the same problem is solve up to Reynolds numbers 5000 by employing the best of the found interpolation strategy from the previous results. The initial guess value in the algorithm is set to be equal to the obtained solution at a lower Re .

A square cavity filled with an incompressible, isothermal and Newtonian fluid is considered. The flow field is due to the motion of the upper wall located at $x_2 = L$, with a prescribed velocity $u_1 = U$ and $u_2 = 0$. The boundary conditions at the remaining walls are given by a zero velocity, i.e. $u_i = 0$ with $i = 1, 2$, and the characteristic Reynolds number is defined by $Re = \frac{UL}{\nu}$, where ν is the kinematic viscosity.

5.1 Comparison among interpolation strategies

Non-uniform meshes of 21×21 , 41×41 and 51×51 Control Volumes (CV) are used for the numerical simulations of the cases of $Re = 100, 400$ and 1000 , respec-

tively, with refined meshes near the boundaries. The results are compared with Ghia, Ghia, and Shin (1982) benchmark solutions. The shape parameter values for the velocity and vorticity MQ functions are kept constant during the solution procedure with their values expressed in terms of a subdomain characteristic length (h) according to $c_i = d_i h$, where d_i is a proportional factor and $i = v, \omega$ for the velocity and vorticity, respectively. For each interpolation strategy, mesh and Reynolds number the shape parameter is found by a qualitative assessment between the obtained numerical result and the benchmark solution. The selected values for d_i are reported for each of the obtained results.

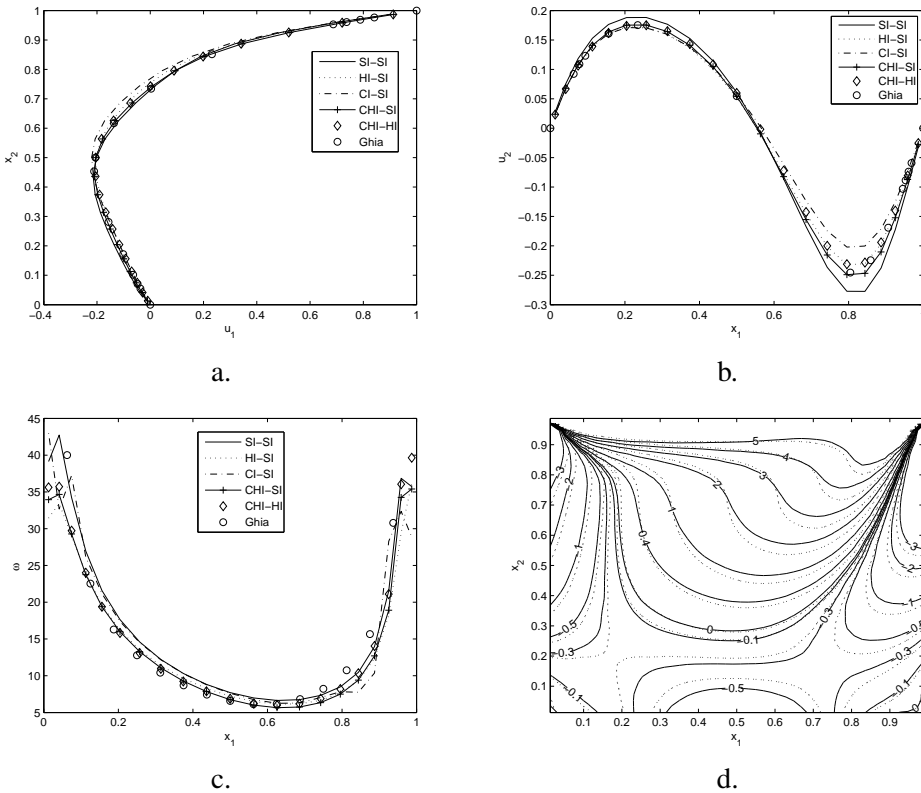


Figure 2: Lid-driven cavity results at $Re = 100$: a. u_1 velocity at line $x_1 = 0.5$, b. u_2 velocity at line $x_2 = 0.5$, c. vorticity values at line $x_2 = 1.0$, d. Vorticity contours using the CHI-SI (---) and SI-SI (...) strategies

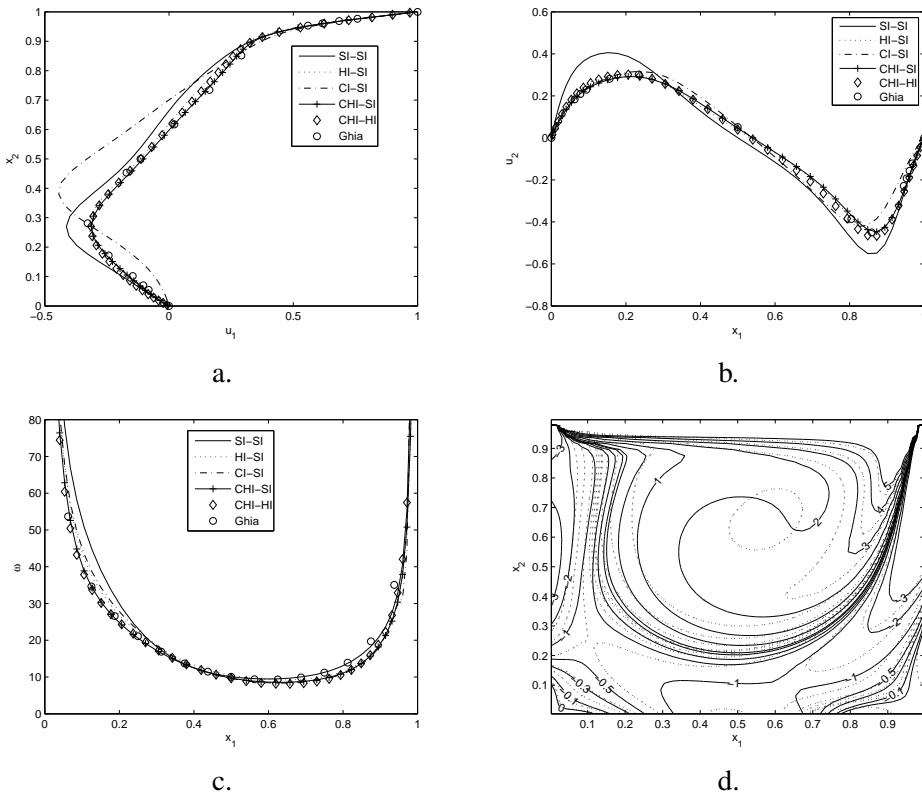


Figure 3: Lid-driven cavity results at $Re = 400$: a. u_1 velocity at line $x_1 = 0.5$, b. u_2 velocity at line $x_2 = 0.5$, c. vorticity values at line $x_2 = 1.0$, d. Vorticity contours using the CHI-SI (--) and SI-SI (...) strategies

At $Re = 100$, acceptable results were obtained by the use of the HI-SI, CHI-SI and CHI-HI interpolation strategies. The corresponding velocity profiles at the central lines of the domain, horizontal and vertical, are shown in Figures 2 a. and 2 b, while vorticity values along the line $x_2 = 1.0$ and the vorticity contours across the cavity are shown in Figures 2 c. and 2 d, respectively. The best overall results were found by using the values of the shape parameters; $d_v = 5.0$ and $d_\omega = 4.0$ for the HI-SI strategy, $d_v = 6.0$ and $d_\omega = 8.0$ for the CHI-SI and $d_v = 8.0$ and $d_\omega = 4.0$ for the CHI-HI. By using the best values of the shape parameter on the CI-SI and SI-SI strategies, the obtained u_1 profile is slightly underestimated, while larger discrepancies on the predicted u_2 velocity profile are observed, similar behaviour

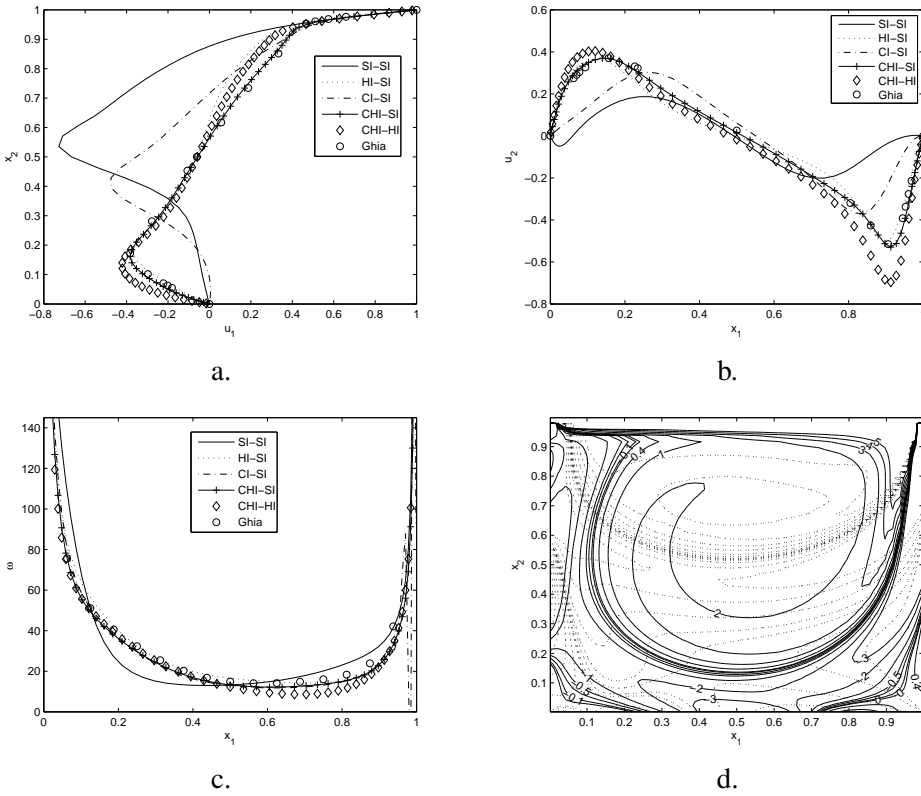


Figure 4: Lid-driven cavity results at $Re = 1000$: a. u_1 velocity at line $x_1 = 0.5$, b. u_2 velocity at line $x_2 = 0.5$, c. vorticity values at line $x_2 = 1.0$, d. Vorticity contours using the CHI-SI (---) and SI-SI (...) strategies

is observed in the obtained values of the vorticity along the line $x_2 = 1.0$. Figure 2 d. presents the comparison between the vorticity contours computed by the CHI-SI strategy (continuous line) and the SI-SI (points), which are, respectively, the best and the worst obtained results.

In the cases of $Re = 400$ and $Re = 1000$, the observed behaviour of the different interpolation strategies was similar to the previous case, with the best results always obtained when using the HI-SI and CHI-SI strategies, being the results predicted by the CHI-SI in the two cases almost identically to the benchmark solutions. However as the magnitude of the Reynolds number increases, the discrepancy between the obtained results with the other schemes, i.e. SI-SI, CI-SI and CHI-HI, and the

benchmark solutions were higher. In both cases, $Re = 400$ and $Re = 1000$, with the set of shape parameters used, no acceptable results were found with the use of the CI-SI and SI-SI strategies.

For $Re = 400$, the best solutions were obtained for the set of parameters; $d_v = 6.0$ and $d_\omega = 5.5$ for the HI-SI, $d_v = 6.0$ and $d_\omega = 8.0$ for the CHI-SI and $d_v = 9.0$ and $d_\omega = 4.0$ for the CHI-HI. The results for this case are reported in Figure 3, where the obtained velocity profiles and vorticity distributions are shown.

The obtained velocity profiles and vorticity distributions, for the case of $Re = 1000$, are shown in Figures 4. Of the tested strategies, the best results were obtained again with the HI-SI and CHI-SI approaches, with shape parameters $d_v = 5.0$ and $d_\omega = 4.5$, and $d_v = 5.0$ and $d_\omega = 8.0$, respectively. The best results with the CHI-HI strategy was found for values of $d_v = 4.2$ and $d_\omega = 1.2$, showing slightly discrepancies in the obtained u_1 and u_2 velocities, as well as the vorticity distribution, in comparison with the reported values of the benchmark solution. Employing the Hermitian interpolation (CHI-HI) for the vorticity approximation seems to be an inadequate strategy for high Reynolds numbers. In this case, the local vorticity interpolation matrix becomes too ill-conditioned before reaching a shape parameter value that can produce accurate results, requiring the use of sophisticated solver which is not the intention of this work. Furthermore, the CHI-HI needs a double iteration strategy (to update the PDE operator M_x) that reduces the computational efficiency of the algorithm.

The main difference between the HI-SI, CHI-SI and CHI-HI strategies and the SI-SI and CI-SI schemes is the presence of the vorticity nodal values in the velocity interpolation. In the HI or CHI for the velocity approximation, the PDE operator L_x from equation (15) allows to express the velocity values and its gradient in terms of the vorticity nodal values. Finally, the importance of applying the conservative interpolation is shown by comparing the obtained results with the HI-SI and the CHI-SI strategies, with always more accurate solutions with the use of the CHI-SI strategy. According to the above analysis, the best and more efficient strategy is the CHI-SI local interpolation scheme, showing almost identical solution than the benchmark solution for each of the Reynolds numbers considered.

5.2 High Reynolds Numbers solutions

In this section, the proposed CVRBF method is used to solve the two-dimensional lid-driven cavity problem at $Re = 1000$, 3200, and 5000. Following our previous analysis of the different local interpolation strategies, in this section the conservative and Hermitian interpolation is employed for approximating the velocity components while a simple interpolation is used in the vorticity case, i.e. the CHI-SI strategy, which always produced the best results in the cases previously consid-

ered. Non-uniform meshes refined towards the walls are used, with 61×61 CV elements in the case of $Re = 1000$, and 81×81 for $Re = 3200$ and $Re = 5000$. The shape parameter were respectively; $d_v = 8.0, d_\omega = 12.0$; $d_v = 6.3, d_\omega = 10.0$ and $d_v = 6.5, d_\omega = 10.0$ for $Re = 1000, 3200$, and 5000 . As before, the obtained results are compared to those reported by Ghia, Ghia, and Shin (1982).

The $Re = 1000$ case is solved again using this time a 61×61 mesh. The velocity profiles shown in Figure 5 a. are similar to those obtained before using a 51×51 mesh. However by using the more refine mesh, the vorticity values along the line $x_2 = 1.0$ and the vorticity contours presented in Figure 6 a. are much closer to the results reported by Bruneau and Saad (2006); Ghia, Ghia, and Shin (1982); Goyon (1996), and Clercx (1997).

Simulations at $Re = 3200$ and $Re = 5000$ are used as more demanding test for the robustness of the proposed CVRBF approach. In both cases, with only a mesh of 81×81 CV elements, the obtained solutions for the velocity components (Figure 5 b. and c.) and the vorticity field (Figure 6 b. and c.) are in good agreement with the benchmark solutions.

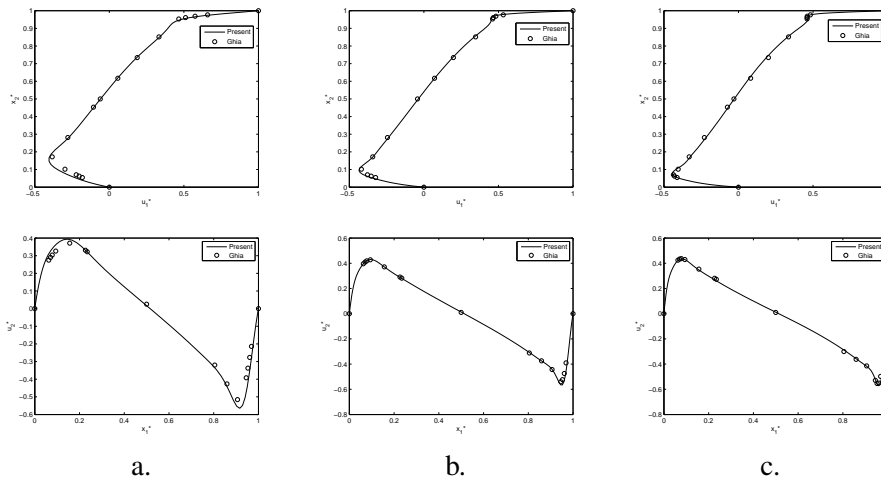


Figure 5: u_1 and u_2 velocity profiles in lines $x_1 = 0.5$ and $x_2 = 0.5$: a. $Re = 1000$, b. $Re = 3200$, c. $Re = 5000$

The results shown in this section for the cases of $Re = 1000, 3200$, and 5000 are as good as or better than some of the most accurate numerical results previous reported in the literature using high order numerical schemes. See for example

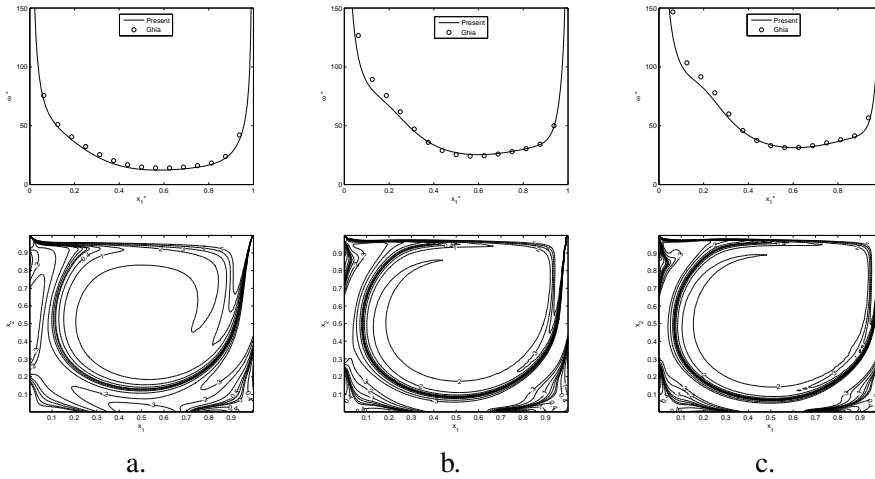


Figure 6: Vorticity behaviour at line $x_2 = 1.0$ and vorticity contours: a. $Re = 1000$, b. $Re = 3200$, c. $Re = 5000$

the works of; Kobayashi, Pereira, and Pereiraz (1999), Wei, Ya-li, and Ru-xun (2009) and Piller and Stalio (2004) where high order CV schemes are reported, Liu and Leung (2001) for a high order FEM, Sanyasiraju and Chandhini (2008) and Bourantas, Skouras, Loukopoulos, and Nikiforidis (2010) where local RBF collocation schemes are used and Bruneau and Saad (2006) where a very dense FD solutions are reported. It is interesting to observe that the results for the $Re = 1000$ case reported in those works, showing similar accuracy than the result for the same Reynolds number reported here, require the use of computational grids that are significant more dense than the one used in our case, except in the case of Piller and Stalio result.

Piller and Stalio's result for $Re = 1000$ obtained with a CV spectral-like compact scheme (sixth order scheme) requires only a mesh of 20×20 elements to achieve similar accuracy to the one reported here with 51×51 elements. However, the compact scheme on staggered grid used in Piller and Stalio's work employed a coordinate transformation between the physical and a computational space, a semi-implicit time stepping scheme that leads to linear systems with $2N$ unknowns for each physical variable with N as the number of CV elements, and in the case of using a coarse grid, as the one used for the $Re = 1000$ result, needs the use of compact high order filtering scheme to damp spurious oscillations (wiggles) when central defined interpolation stencils are used. On the other hand, our scheme,

which is also based on central defined interpolation stencils, is defined only in the the physical space, with N unknowns for each physical variable, instead of $2N$, and never needs the use of any filtering scheme (for more detail about the stability of the type of CVRBF approach used in this work when dealing with scalar transport equations see Orsini, Power, Morvan, and Lees (2010)). It is important to comment that in Piller and Stalio's approach, it is not necessary to use any filtering scheme to obtain stable solution when fine enough grids are used, as is the case of their reported solution for $Re = 5000$ with 160×160 and 320×320 elements. The Piller and Stalio's $Re = 5000$ result with the use of those dense meshes are equivalent to our solution for the same Reynolds number with only 81×81 mesh and also without the need of any filtering scheme.

It is also important to point out that in our solutions the shape parameters used are not necessary the optimal ones, which were selected by the previously mentioned simple geometric relation. It is well known that by selecting the optimal values of the shape parameters in a MQ interpolation and having variable values along the computational domain it is possible to improve the accuracy of the local interpolation by at least one or two order of magnitude (see Bayona, Moscoso, and Kindelan (2011)). Consequently, it is expected that by properly selecting the shape parameters of the local interpolation our results can be substantially improved, however this is beyond the scope of the present work. On the other hand, it is also possible to improve the present solution by using larger interpolation stencils including more than the CV centre points of just the near neighbours CV elements, as used in the present work, with the corresponding increase in computational cost and possible worsening of the conditioning of the interpolation matrices.

6 Conclusions

An implementation of the CV-RBF scheme for the numerical solution of non-linear coupled system of PDEs is presented with application to 2D driven cavity flow at different Reynolds numbers, achieving excellent results with the use of course meshes up to Reynolds numbers 5000. Different velocity and vorticity interpolation strategies at the local level are proposed and tested, from which the best alternative is selected among different tested options. Interpolation strategies where the velocity approximation is not coupled to the vorticity nodal values (simple and conservative) fail for $Re > 400$, requiring the use of coupled interpolations for larger Reynolds numbers. A Hermitian interpolation for the vorticity field is not a suitable strategy since the obtained interpolation matrix becomes ill-conditioned before reaching an adequate shape parameter value and the requirement of double-iteration scheme, which is computationally inefficient. Therefore, for the solution at $Re > 400$ a Hermitian and Conservative interpolation is used for the velocity

components together with a Simple interpolation for the vorticity field. The evaluation of the vorticity boundary values is avoided by coupling the vorticity and velocity governing equations through the local interpolation scheme. Other features of the CV-RBF method such as the mesh independency of the interpolation scheme and the versatility to deal with different kind of boundary condition can be explored in future applications.

References

Abgrall, R. (1994): On essentially Non-Oscillatory Schemes on Unstructured Meshes. *Journal of Computational Physics*, vol. 114, no. 1, pp. 45–58.

Bayona, V.; Moscoso, M.; Kindelan, M. (2011): Optimal constant shape parameter for multiquadric based rbf-fd method. *Journal of Computational Physics*, vol. 230, pp. 7384–7399.

Bourantas, G. C.; Skouras, E. D.; Loukopoulos, V. C.; Nikiforidis, G. C. (2010): Numerical solution of non-isothermal fluid flows using local radial basis functions (lrbf) interpolation and a velocity-correction method. *J. Comput. Methods Eng. Sci. Mech.*, vol. 64, pp. 187–212.

Brown, D. (2005): On approximate cardinal preconditioning methods for solving pdes with radial basis functions. *Engineering Analysis with Boundary Elements*, vol. 29, pp. 343–353.

Bruneau, C. H.; Saad, M. (2006): The 2d lid-driven cavity problem revisited. *Computers & Fluids*, vol. 35, pp. 326–348.

Clercx, H. J. H. (1997): Spectral solver for the navier stokes equations in the velocity-vorticity formulation for flows with two nonperiodic directions. *Journal of Computational Physics*, vol. 137, pp. 186–211.

Divo, E.; Kassab, K. (2006): An efficient localised radial basis function collocation method for fluid flow and conjugate heat transfer. *J. Heat Transfer*, vol. 212, pp. 99–123.

Dumbser, M.; Kaser, M. (2007): Arbitrary high order non-oscillatory finite volume schemes on unstructured meshes for linear hyperbolic systems. *Journal of Computational Physics*, vol. 211, pp. 693–723.

Dworkin, S. B.; Bennett, B. A. V.; Smooke, M. D. (2006): A mass-conserving vorticity-velocity formulation with application to nonreacting and reacting flows. *Journal of Computational Physics*, vol. 215, pp. 430–447.

Fasshauer, F. E. (1997): Solving partial differential equations by collocation with radial basis functions. *Surface Fitting and Multiresolution Methods*, pp. 131–138.

Florez, W. F.; Power, H. (2002): Drm multidomain mass conservative interpolation approach for the bem solution of the two-dimensional navier-stokes equations. *Computers & Mathematics with Applications*, vol. 43, no. 3-5, pp. 457–472.

Fornberg, B.; Flyer, N. (2005): Accuracy of radial basis function interpolation and derivative approximations on 1-d infinite grids. *Advances in Computational Mathematics*, vol. 23, no. 1, pp. 5–20.

Ghia, U.; Ghia, K. N.; Shin, C. (1982): High-re solutions for incompressible flow using the navier-stokes equations and a multigrid method. *Journal of Computational Physics*, vol. 48, no. 3, pp. 387–411.

Goyon, O. (1996): High-reynolds number solutions of navier-stokes equations using incremental unknowns. *Comput. Method. Appl. M*, vol. 130, pp. 319–335.

Hribersek, M.; Skerget, L. (2005): Boundary domain integral method for high reynolds viscous fluid flows in complex planar geometries. *Computer methods in applied mechanics and engineering*, vol. 194, no. 1, pp. 4196–4220.

Huang, C. S.; Lee, C. F.; Cheng, A. H. D. (2007): Error estimate, optimal shape factor, and high precision computation of multiquadric collocation method. *Engineering Analysis with Boundary Elements*, vol. 31, no. 1, pp. 614–623.

Huang, H.; Li, M. (1997): Finite difference approximation for the velocity-vorticity formulation on staggered and non-staggered grids. *Computers & fluids*, vol. 26, no. 1, pp. 59–82.

Jayantha, P. A.; Turner, I. W. (2005): A second order control-volume-finite-element least-squares strategy for simulating diffusion in strongly anisotropic media. *Journal of Computational Mathematics*, vol. 23, no. 1, pp. 1–16.

Jumarhon, B.; Amini, S.; Chen, K. (2000): The hermite collocation method using radial basis functions. *Engineering Analysis with Boundary Elements*, vol. 24, no. 7-8, pp. 607–611.

Kansa, E. J. (1990): Multiquadrics -a scattered data approximation scheme with applications to computational fluid dynamics-ii solution to parabolic, hyperbolic and elliptic partial differential equations. *Computers & Mathematics with applications*, vol. 19, no. 8-9, pp. 127–145.

Kansa, E. J.; Hon, Y. C. (2000): Circumventing the ill- conditioning problem with multiquadric radial basis functions: Applications to elliptic partial differential equations. *Computers & Mathematics with applications*, vol. 39, no. 1, pp. 123–137.

Kobayashi, M. H.; Pereira, J. M. C.; Pereiraz, J. C. F. (1999): A conservative finite-volume second-order-accurate projection method on hybrid unstructured grids. *Journal of Computational Physics*, vol. 150, pp. 40–75.

- LaRocca, A.; Hernandez, A.; Power, H.** (2005): Radial basis functions hermite collocation approach for the solution of time dependent convection-diffusion problems. *Engineering Analysis with Boundary Elements*, vol. 29, no. 4, pp. 359–370.
- LaRocca, A.; Power, H.** (2008): A double boundary collocation hermitian approach for the solution of steady state convection-diffusion problems. *Computers & Mathematics with applications*, vol. 55, no. 9, pp. 1950–1960.
- Lee, C.; Liu, X.; Fan, S.** (2003): Local multiquadric approximation for solving boundary value problems. *Comput. Mech.*, vol. 30, pp. 396–409.
- Ling, L.; Schaback, R.** (2004): On adaptive unsymmetric meshless collocation. *Proceedings of the 2004 international conference on computational and experimental engineering and sciences*.
- Liu, C. H.; Leung, D. Y. C.** (2001): Development of a finite element solution for unsteady navier-stokes equations using projection method and fractional θ -scheme. *Comput. Meth. Appl. Mech. Eng.*, vol. 190, pp. 4301–4317.
- Liu, F.; Turner, I. W.; Anh, V.** (2002): An unstructured mesh finite volume method for modelling saltwater intrusion into costal aquifers. *Appl. Math. Comput.*, vol. 9, pp. 391–407.
- Lo, D. C.; L.Young, D.; Tsai, C. C.** (2007): High resolution of 2d natural convection in a cavity by the dq method. *Journal of Computational and Applied Mathematics*, vol. 203, no. 1, pp. 219–236.
- Madych, W. R.** (1992): Miscellaneous error bounds for multiquadric and related interpolators. *Journal of Computational and Applied Mathematics*, vol. 24, pp. 121–138.
- Madych, W. R.; Nelson, S. A.** (1990): Multivariate interpolation and conditionally positive definite functions. *Mathematics of Computation*, vol. 54, no. 1, pp. 211–230.
- Manzini, G.; Putti, M.** (2007): Mesh locking effects in the finite volume solution of 2-d anisotropic diffusion equations. *Journal of Computational Physics*, vol. 220, no. 2, pp. 751–771.
- Moroney, T. J.; Turner, I. W.** (2006): A finite volume method based on radial basis functions for two-dimensional nonlinear diffusion equations. *Applied Mathematical Modelling*, vol. 30, no. 10, pp. 1118–1133.
- Moroney, T. J.; Turner, I. W.** (2007): A three dimensional finite volume method based on radial basis functions for the accurate computational modelling of nonlinear diffusion equations. *Journal of Computational Physics*, vol. 225, no. 2, pp. 1409–1426.

Orsini, P.; Power, H.; Morovan, H. (2008): Improving volume element methods by meshless radial basis function techniques. *CMES: Computer modelling in Engineering and Sciences*, vol. 769, no. 1, pp. 1–21.

Orsini, P.; Power, H.; Morvan, H.; Lees, M. (2010): An implicit upwinding volume element methods based on meshless radial basis function techniques for modelling transport phenomena. *Int. J. Numer. Methods Eng.*, vol. 81, pp. 1–27.

Pascasio, G.; Napolitano, M. (1996): A staggered-grid finite volume method for the vorticity-velocity equations. *Computers & Fluids*, vol. 25, no. 4, pp. 433–446.

Perron, S.; Boivin, S.; Herard, J. M. (2004): A finite volume method to solve the 3d navier-stokes equations on unstructured collocated meshes. *Computers & Fluids*, vol. 33, no. 1, pp. 1305–1333.

Piller, M.; Stalio, E. (2004): Finite-volume compact schemes on staggered grids. *Journal of Computational Physics*, vol. 197, pp. 299–340.

Qian, L.; Veza, M. (2001): A vorticity-based method for incompressible viscous flows. *Journal of Computational Physics*, vol. 172, no. 1, pp. 515–542.

Sanyasiraju, Y. V. S. S.; Chandhini, G. (2008): Local radial basis function based gridfree scheme for unsteady incompressible viscous flows. *Journal of Computational Physics*, vol. 227, no. 20, pp. 8922–8948.

Sarler, B.; Vertnik, R. (2006): Meshless explicit local radial basis function collocation methods for diffusion problems. *Computers & Mathematics with Applications*, vol. 51, pp. 1269–1282.

Schaback, R. (1995): Multivariate interpolation and approximation by translates of basis functions. *Approximation Theory*, vol. 8, pp. 1–8.

Skerget, L.; Rek, Z. (1995): Boundary integral domain method using a velocity-vorticity formulation. *Journal of Computational Physics*, vol. 15, no. 1, pp. 359–370.

Truscott, S. L.; Turner, I. W. (2004): An investigation of the accuracy of the control volume-finite element based on triangular prismatic elements for simulating diffusion in anisotropic media. *Numerical Heat Transfer, Part B: Fundamentals*, vol. 46, no. 1, pp. 45–98.

Vidovic, D.; Segal, A.; Wesseling, P. (2004): A superlinearly convergent finite volume method for the incompressible navier stokes equations on staggered unstructured grids. *Journal of Computational Physics*, vol. 198, no. 1, pp. 159–177.

Wei, G.; Ya-li, D.; Ru-xun, L. (2009): The finite volume projection method with hybrid unstructured triangular collocated grids for incompressible flows. *J. Hydrodyn. Ser. B*, vol. 21, pp. 201–211.

Wright, G.; Fornberg, B. (2006): Scattered node compact finite difference-type formulas generated from radial basis functions. *Journal of Computational Physics*, vol. 212, no. 1, pp. 99–123.

Ye, T.; Mittal, R.; Udaykumar, H. S.; Shyy, W. (1999): An accurate cartesian grid method for viscous incompressible flows with complex immersed boundaries. *Journal of Computational Physics*, vol. 156, no. 1, pp. 209–240.

Young, D. L.; Liu, Y. H.; Eldho, T. I. (2000): A combined bem-fem model for the velocity-vorticity formulation of the navier stokes equations in three dimensions. *Engineering Analysis with Boundary Elements*, vol. 24, no. 1, pp. 307–316.

Zunic, Z.; Hribersek, M.; Skerget, L.; Ravnik, J. (2007): 3-d boundary element-finite element method for velocity-vorticity formulation of the navier-stokes equations. *Engineering Analysis with Boundary Elements*, vol. 31, no. 1, pp. 259–266.